Transport, Analyte Detection, and Opto-Electronic Response of p-Type CuO Nanowires

Benjamin J. Hansen,[†] Nikolai Kouklin,[‡] Ganhua Lu,[§] I-Kuan Lin,[†] Junhong Chen,*[,§] and Xin Zhang*[,†]

Department of Mechanical Engineering, Boston University, Boston, Massachusetts 02215, Department of Electrical Engineering, Department of Mechanical Engineering, University of Wisconsin-Milwaukee, Milwaukee, Wisconsin 53211

Received: September 13, 2009; Revised Manuscript Received: January 11, 2010

In this article, we introduce and provide details on a large-scale, cost-effective pathway to fabricating ultrahigh dense CuO nanowire arrays by thermal oxidation of Cu substrates in oxygen ambient. The CuO nanowires that are produced at ~500 °C for ~150 min feature an average length and diameter of ~15 μm and ~200 nm, respectively. The room temperature device-related characteristics such as transport, analyte detection and opto-electronic response of individual CuO nanowires have been probed by fabricating single CuO nanowire devices with the use of lift-off photolithographical techniques. The experiments confirm that as-grown nanowires are of p-type, have a band gap of ~1.4 eV, and show strong sensitivity to both NO_2 and NH_3 gases. The devices also showed strong response to white light with device responsivity approaching ~8 A/W for optical power densities of only ~1 mW/cm^2. Additionally, a complex interaction of photoproduced electron−hole pairs with the surface-originating chemisorbed agents including O_2 and NO_2 is found to drastically affect the gas sensitivity of CuO nanowire-based devices, where photoinduced adsorption of the analyte enhances the device response.

1. Introduction

Tremendous ongoing efforts have been devoted to exploring the fabrication and characterization of novel nanostructures for applications in next-generation solid-state devices, optical, and analyte sensors. In particular, semiconductor nanowires (NWs) and carbon nanotubes (CNTs) have emerged as promising multifunctional materials that can be utilized as both wiring and device elements, providing a pathway to building a variety of hybrid nanoelectronic, nano-optoelectronic, nanomechanical, and electro-chemical devices.[1–5] As a result, there has been a sustained effort to produce semiconducting NWs in different materials systems and with drastically improved and novel device functionalities. In part, this has also catalyzed the search for new low-cost approaches to synthesizing quality nanostructures in metal-oxides such as ZnO, In_2O_3, TiO_2, and CuO with the latter remaining less studied and explored.

To realize the full potential of these novel NW components for device applications, new methods enabling a systematic and controlled modification of their intrinsic characteristics are needed. Various growth techniques have been investigated: vapor−liquid−solid growth,[6] metal organic vapor phase epitaxy,[7] vapor−solid growth,[8] and wet chemical methods.[9] Many of these growth methods suffer from complex procedures, expensive technologies, and/or low output, and often require a catalyst such as Au. Here we explore an alternative approach for the large scale and low-cost growth of p-type semiconducting cupric oxide (CuO) NWs by a method of direct oxidation of copper substrates.[10,11] The simplicity of the direct oxidation technique, together with its high NW yield and potential for controllability, makes it an attractive avenue for future device development and use.

Among the various semiconductor NWs currently under investigation, metal oxide NWs are a highly important class of materials in both current and future device technologies. Their potential applications are far reaching and include chemical and optical sensing, solid-state lighting, optical switches, catalysis, transparent conductive films, solar-cells, piezoelectronics, and electromechanical devices.[12] Among the metal oxides, CuO has the unique property of being intrinsically p-type and with a low band gap (1.2−2.0 eV) making it the lowest bandgap metal oxide semiconductor available.[13,14] The low band gap of CuO could prove it useful in photodetection and optical switching applications in the visible range where other metal oxides with their larger band gaps fail to perform.[15] In addition, the intrinsic p-type characteristic of CuO and its counterpart cuprous oxide (Cu_2O) may provide a unique route for forming p-n heterojunctions with other metal-oxide NWs such as those in ZnO and TiO_2 that exhibit predominantly n-type doping and for which p-type doping has proven to be difficult. Indeed, p-n heterojunctions of this type have been explored in thin-film technology to enhance gas sensing selectivity and sensitivity (CuO/ZnO),[16] and to create light-emitting diodes (LEDs) and photovoltaic cells (Cu_2O/ZnO).[17]

Some efforts have been made to use CuO NWs in applications such as gas sensors[18–20] and field emitters.[21] For instance, Chen et al. investigated the H_2S sensing properties of two vertically aligned arrays of CuO nanowires mechanically interconnected. However, the intrinsic physics associated with a single NW could be lost due to averaging effects in a NW array. In addition, little is offered in previous work about CuO NW gas sensors[18–20] in terms of the mechanisms contributing to the overall sensing behavior. Furthermore, no work is available on the optical sensing characteristics of CuO NWs which can significantly

* To whom correspondence should be addressed. E-mail (J.C.) jhchen@uwm.edu; (X.Z.) xinz@bu.edu.
[†] Boston University.
[‡] Department of Electrical Engineering, University of Wisconsin-Milwaukee.
[§] Department of Mechanical Engineering, University of Wisconsin-Milwaukee.

10.1021/jp908850j
Published on Web 01/26/2010

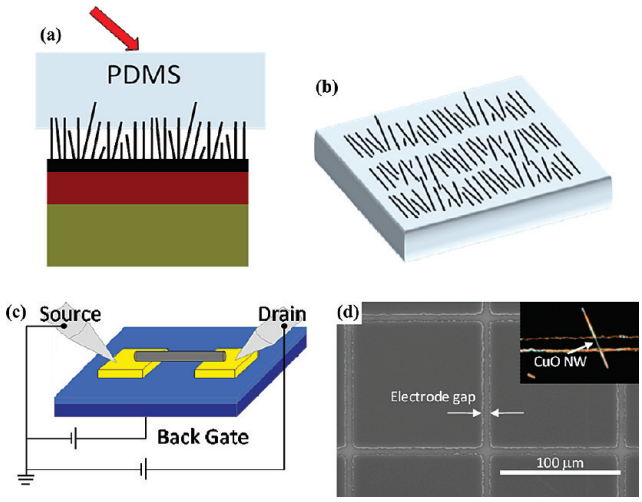

Figure 1. (a,b) Schematic of the clean transfer of NWs from the growth substrate to PDMS. (c) A schematic of a single NW-FET. (d) An SEM image of 100 × 100 μm square electrode array with 5 μm spacing (the inset is dark-field image of a single CuO NW bridging two electrodes with a 5 μm gap).

contribute to the understanding of the surface states and molecular absorption processes, thus can provide insights into the general behavior of p-type metal-oxide NWs. Past studies have been focused on n-type metal-oxide NWs for light and gas sensing applications where the interaction of analyte molecules (O_2 and NO_2) with photogenerated charge carriers is intimately related.[22] To our knowledge, no similar works are available for p-type metal-oxides. As the research community is now beginning to achieve p-type doping of typically n-type metal-oxide NWs for novel optical devices,[23] understanding the surface interactions of p-type metal-oxides will be essential. Here, we demonstrate the fabrication of single CuO NW devices and the use of these devices to explore the electrical transport, anlalyte sensing, and opto-electronic characteristics of this p-type metal-oxide. Importantly, our results indicate that light irradiation above the NW bandgap of p-type CuO results in analyte absorption, thus offering a novel way to modulate the gas sensitivity of p-type metal-oxide based sensors. The light-induced analyte absorption could be a unique characteristic of p-type metal oxides whereas light irradiation of n-type metal oxides results in the molecular desorption of the analyte species.[22]

2. Experimental Section

2.1. Growth of CuO NW Arrays. The large scale growth of high density CuO nanowire arrays is accomplished by direct oxidation of copper. In this study, copper foil (5Ns, 0.2 mm thick) was first cleaned with ethanol, rinsed with deionized (DI) water, dried in dry air, cleaned with 1.5 M HCl, rinsed with DI water, and once again dried in dry air. The substrate was then oxidized at 500 °C in a pure O_2 gas flow for 150 min as described in detail elsewhere.[10]

2.2. Transfer of NWs. To transfer the NWs cleanly from the copper/(copper oxide) surface without removing the amorphous oxide layer, a thin piece (~1 mm) of polydimethylsiloxane (PDMS) is gently pressed against the top of the oxide and then removed (Figure 1a,b). The PDMS with high density NWs on the surface is placed in a small amount of ethanol and gently ultrasonicated to remove the NWs from the PDMS. The NWs, now dispersed in ethanol, can be deposited onto the electrode grids. Alternatively, the PDMS substrate with high density NWs can be directly used for optical measurements such as UV−visible absorption. The PDMS substrate/NW removal technique can be broadly applied to many other NW growth processes.

2.3. Fabrication of Single NW Devices. Standard photolithography techniques were used to fabricate single NW devices. The platform of the NW device is a single nanowire field effect transistor (NW-FET) shown in Figure 1c, which is often used to study the electrical transport characteristics and sensing properties of nanowires and nanotubes.[24,25]

A 4 in. p-type Si (0−100 Ω) wafer with a thermally grown 150 nm SiO_2 layer (University Wafer) was cleaned and the backside SiO_2 layer was removed using a 6:1 buffered oxide etchant (BOE). Next, standard photolithography and metal deposition techniques were used to pattern multiple 1 × 1 cm cells of 100 × 100 μm square Ag electrodes with 5 or 10 μm spacing between each electrode (Figure 1d).

After depositing the NWs onto the electrode array, a high resolution optical microscope (500× or 1000×) is used to locate a single NW that bridges two of the electrodes (Figure 1d, inset), and the exact location is recorded (electrode column and row numbers). To improve the electrical contact, a top electrode layer is deposited using the same photolithography and metal deposition techniques used to deposit the bottom electrodes. This is an easy and robust technique for fabricating and studying single nanowire devices and can be expanded upon to consistently fabricate NW based Schottky devices.

2.4. Characterization of NWs and Single NW Devices. Optical microscopy and scanning electron microscopy (SEM) (Hitachi S 4800) were used during the course of the single NW device fabrication. Morphology and crystalline structure of the as-produced NWs were analyzed using a Hitachi H 9000 NAR transmission electron microscope (TEM) through bright-field TEM and high-resolution TEM (HRTEM) imaging and selected area diffraction (SAD). The electrical measurements of single CuO NW devices were carried out using a probe station equipped with an HP/Agilent 4155 Semiconductor Parameter Analyzer.

A Cary UV−vis spectrophotometer under transmission mode at room temperature was used for UV−vis absorption measurements. The PDMS sample with high-density NWs on the surface was mounted to a slide with a 0.5 mm aperture. The resolution was set to 0.5 nm with a 3 s averaging time. A clean portion of the PDMS without any NWs was used as the background.

The photo-$I-V$ characteristics were obtained with the help of a source-meter system (Keithley 2600) operating in conjunction with a reflection mode Mitutoyo optical microscope and probe station. The single NW device was located with the microscope and centered in the view. A variable white light source then acted as the photon source for the experiment, where the light intensity was measured using a commercial photodiode and hand-held readout system (Si-detector, S120B from Thorlabs).

The gas sensing properties of a single CuO NW device was characterized at room temperature for the detection of low-concentration gases including NO_2 (100 ppm) and NH_3 (1%) diluted in dry air. Gases were detected by measuring the change in the electrical conductance of the CuO NW in response to the exposed gaseous environment, similar to the procedure that we previously used to characterize CNT-based sensors.[26] Under a typical experiment, a constant voltage was applied to the NW and the output current was recorded in 1 s increments utilizing a Keithley 2602 source meter and LabView data acquisition. One sensing cycle consisted of introducing a flow of 2 lpm of

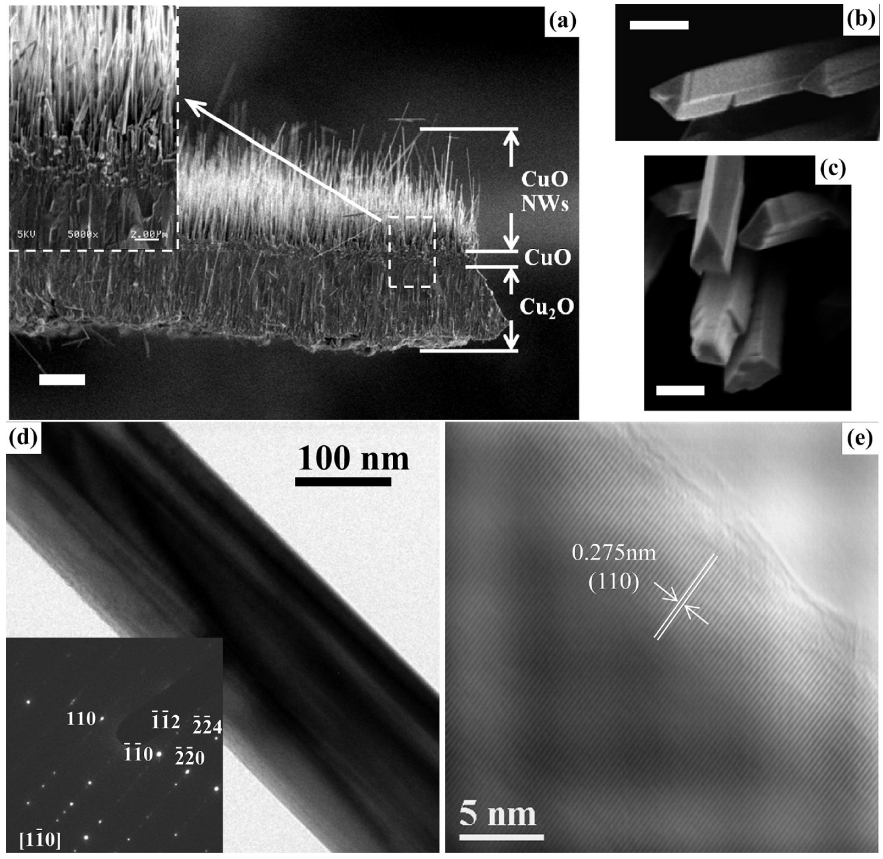

Figure 2. (a) An SEM image of the copper oxide flake removed from an oxidized copper substrate (10 μm scale bar).[10] (b,c) High-resolution SEM images of CuO NW cross sections (200 nm scale bar). TEM (d) and HRTEM (e) images of a CuO NW; the inset in (d) is a SAD pattern of the NW.

dry air for 10 min to achieve a baseline, changing to 2 lpm of the (sensing gas)/(air) mixture for 3 min, followed by changing back to 2 lpm of dry air flow for a 15 min sensor recovery. Each experiment consisted of a total of five cycles. To ensure full recovery before testing a new gas, a 24 h period was allowed between experiments. The chamber volume was minimized ($\sim$1 $\times$ 10^{-5} m^3) to reduce the capacitive effect when changing between gaseous environments. Cylinders with certified gas concentrations were obtained from Praxair for the gas sensing experiments.

3. Results and Discussion

3.1. Growth of CuO Nanowire Arrays. The oxidation of copper at intermediate temperatures results in parallel oxide layering structures with the three distinguishable layers identified as an amorphous Cu_2O bottom layer that lies directly above the copper substrate, an intermediate amorphous CuO layer, and a top layer of high-density crystalline CuO NWs, as illustrated in Figure 2a. This is consistent with basic diffusion theory where the concentration of the diffusing species (Cu) decreases with increasing distance from the source (i.e., Cu_2O has a higher concentration of Cu than CuO and hence Cu_2O exists nearest the Cu substrate followed by the CuO phase). Figures 2b and c show high-resolution scanning electron microscopy (SEM) images taken directly above vertically grown NWs, elucidating the faceted nature of the crystals. The geometrical shape of the cross section shows some variation, which indicates a distribution of the NW crystal orientation and suggests multiple preferred growth orientations. This is consistent with the literature that has identified various growth directions of CuO NWs via the direct oxidation method.[10,11,27] Therefore, CuO NWs grown by this method may be limited to applications where anisotropic effects and sample variations are not critical.

Figure 2d is a low-magnification TEM image of a NW grown in pure O_2 from a high-purity Cu foil. The visible stripes along the NW axis are clearly seen with different contrasts and indicate that as-grown NWs have faceted instead of circular cross sections, which is consistent with the SEM observation (Figure 2b,c). The SAD pattern of the NW in the inset of Figure 2d confirms the crystallinity of product nanowires. Figure 2e is an HRTEM image of the NW shown in Figure 2d; lattice spacing analysis by numerical diffractograms gives a value of 0.275 nm, corresponding to the (110) plane of CuO. Combining SAD and HRTEM analyses, the NW growth direction could be identified as [110].

The catalyst free, one-dimensional growth of crystalline CuO is attributed to the anisotropic nature of the crystal surfaces. The crystal plane corresponding to the growth direction (e.g., NW tip) presumably has a higher surface energy and/or chemical activity than the outer faceted surfaces of the NW. Therefore, the oxidation reaction and the subsequent growth, preferentially occurs at the NW tip and results in the continuous growth of a one-dimensional nanostructure.

3.2. Field-Effect Transistor Properties of a Single CuO NW. The platform of the NW device is a single nanowire field effect transistor (NW-FET) (Figure 1c,d) that was used to measure the electrical characteristics of a single CuO NW with a channel length of $\sim$12 μm and a diameter of $\sim$200 nm. The drain-source $I_{ds}-V_{ds}$ curves at different gate voltages (V_g) (Figure 3a) clearly show that the $I_{ds}-V_{ds}$ curves are modulated by V_g and the NW conductance decreases by increasing V_g. This demonstrates the p-type semiconducting behavior of CuO NWs

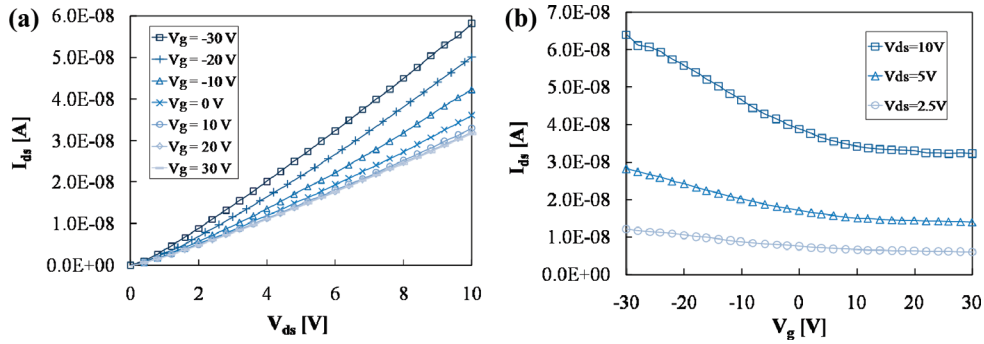

Figure 3. (a) $I_{ds}-V_{ds}$ curves at different gate voltages. (b) $I_{ds}-V_g$ curves with V_{ds} equal to 10, 5, and 2.5 V, respectively.

which is further verified by a transconductance measurement, current (I_{ds}) versus gate voltage (V_g) at different drain voltages (V_{ds}) as presented in Figure 3b. The device shows weak gating effect where the conductance of the NW (I_{ds}/V_{ds}) is modulated by a factor of 2 with V_g sweeping from −30 to 30 V. The weak gating effect of CuO NWs is consistent with the literature[18] while slight variations are likely due to factors such as crystal orientation, defect concentration, free carrier density, and nanowire size, which can eventually be optimized to improve the device response. The NW-FET is a "normally-on" type transistor, presumably with hole-injection from the source metal contacts. As the gate voltage is increased in the positive direction a threshold voltage is reached where the conductance cannot be decreased any further. By drawing two tangents, one through the semilinear portion of the curve at negative V_g and the other through the semihorizontal portion at positive V_g and noting the value of V_g where they cross, a threshold voltage (V_t) is estimated to be ∼9 V. In theory, the NW should be fully depleted of charge carriers for gate voltages at or above V_t.[24,25] The fact that there is still a relatively large amount of current flowing through the NW for $V_g > V_t$ suggests that there is either an additional conduction path, such as photoresist (PR) remaining on the NW surface or a net surface charge.

To realize the full potential of NW components for device applications, new methods enabling a systematic and controlled modification of their intrinsic characteristics are needed. Stoichiometry plays an important role in the optical and electronic properties of materials. It is generally accepted that CuO is metal deficient ($Cu_{1-x}O$) with a corresponding defect equation described as

$$\frac{1}{2}O_2 \leftrightarrow V_{Cu}^{2-} + 2h^+ + O_o;\ K = \frac{[V_{Cu}^{2-}]\cdot[h^+]^2}{p_{o_2}^{1/2}} \qquad (1)$$

where K is a constant, p_{O_2} is the O_2 partial pressure, and $[V_{Cu}^{2-}]$ and $[h^+]$ represent the concentration of copper vacancies and holes, respectively. The existence of copper vacancies results in the production of holes and agrees with the reported minute presence of Cu^{3+} and the p-type semiconducting behavior of CuO.[13,28] According to the defect equation, it is suggested that the concentration of holes and thus the electrical carrier concentration and conductivity of CuO NWs could be controlled by the partial pressure of oxygen during the growth and will be highly sensitive to the presence of absorbed molecules, ideal for chemical and environmental sensing.

3.3. Gas Sensing Properties of a Single CuO NW. The gas sensing properties of a single CuO NW with a diameter of ∼200 nm and channel length of ∼5 μm were characterized at room temperature for the detection of low-concentration gases, 100 ppm NO_2 and 1% NH_3 in dry air. Figure 4a is the current versus time plot (with a device bias of 5 V) for the NO_2 sensing experiment. Contrary to n-type metal oxides,[22] the current and therefore the conductance are found to increase with the introduction of 100 ppm of NO_2. NO_2 has an unpaired electron and is known as a strong oxidizer. Upon NO_2 absorption, similar to that of O_2, charge transfer is likely to occur from the CuO NW to the NO_2 as governed by $NO_2 + e^- \rightarrow NO_2^-$. The electron transfer from the NW to the NO_2 results in lowering of the quasi-Fermi level and thus increased free hole density and enhanced conductance (Figure 4b). In addition, the negatively charged chemisorbed NO_2 molecule at the CuO NW surface may act as a negative gate bias and increase the conductance of the NW.

The sensor sensitivity versus time for the fourth cycle is presented in Figure 4c. The sensor sensitivity is defined as a relative change in the device conductance, $\xi = (G_g - G_a)/G_a$, where G_a is the sensor conductance in air and G_g is that in the target gas. In a typical experiment, in which the CuO nanosensor was exposed to ∼100 ppm NO_2, ξ was around 0.13. The response time constant, defined as the time needed for the sensor conductance, G, to increase by 63.2% from its base value in air to the maximum value in NO_2, was ∼1 min; the recovery time constant, which is the time required for G to decrease by 63.2% from the maximum value in NO_2 to that in air was ∼4.5 min. The slow recovery suggests slow molecular desorption from the NW surface at room temperature. To improve the response and recovery time, semiconductor gas sensors are often heated to above 200 °C to enhance the chemical processes at the surface.[29] However, operating at elevated temperatures limits the application to nonflammable, nonexplosive environments, and increases the complexity of the device and the overall operating cost.

The same device also exhibited sensitivity to NH_3. The current versus time plot (8 V bias) is presented in Figure 4d. In contrast to NO_2, the presence of 1% NH_3 resulted in a decrease in current and conductance. It is well-known that the surface defects of metal oxides function as O_2 adsorption sites. The O_2 molecules adsorbed at these sites act as electron acceptors in the chemisorption process ($O_2 + 2e^- \rightarrow 2O^-$). This results in negatively charged chemisorbed oxygen (O^- or O_2^-) at the surface. The presence of these negatively charged oxygen molecules act as a negatively applied quasi-gate voltage and results in a local accumulation of holes near the surface of the p-type CuO NW. The interaction between the reducing gas (NH_3) and the negatively charged O^- ions has been previously found to follow the reaction pathway $2NH_3 + 3O^- \rightarrow 3H_2O + N_2 + 3e^-$.[30] In this case, the electron transfer from the O^- ions to the NW results in decreased hole density and thus decreased conductance (Figure 4e). In addition, reducing the number of negative O^-

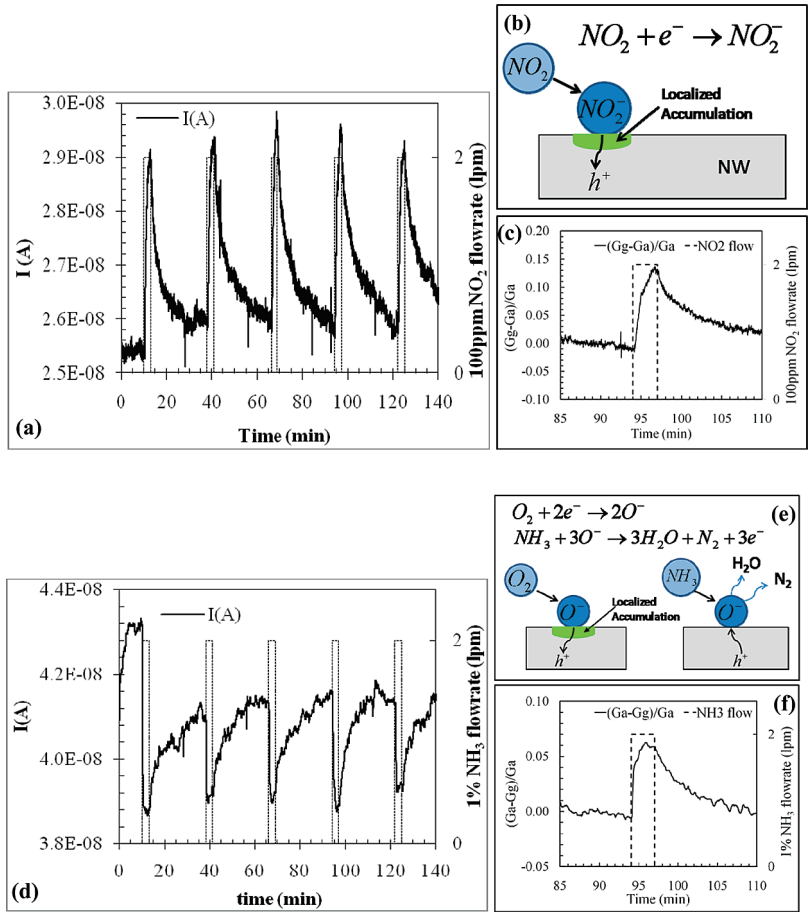

Figure 4. (a) Dynamic response of the CuO NW sensor for room-temperature detection of 100 ppm NO_2; (b) schematic of the proposed NO_2 sensing mechanism; and (c) sensor sensitivity versus time taken from cycle four of the experiment. (d) Dynamic response of the sensor for room-temperature detection of 1% NH_3; (e) proposed NH_3 sensing mechanism; and (f) sensor sensitivity versus time taken from cycle four of the experiment.

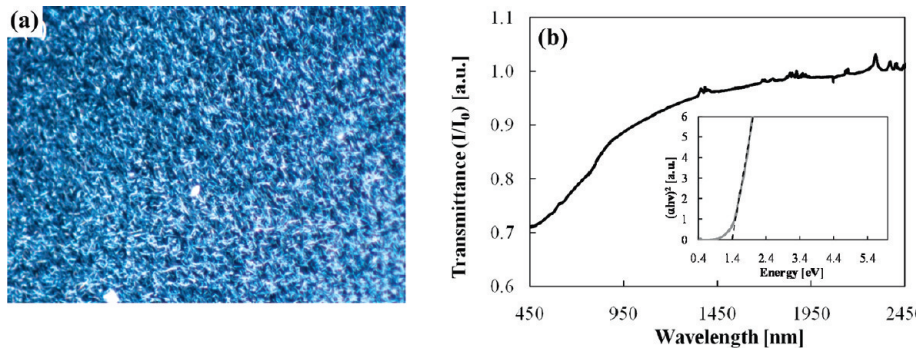

Figure 5. (a) Optical image of the high density NWs on the PDMS substrate; (b) transmittance spectrum of CuO NW array and (inset) optical bandgap fitting.

ions on the surface reduces the magnitude of the negative quasi-gate voltage which in turn decreases the conductivity.

For NH_3, the sensor sensitivity or change in conductance, now defined as $(G_a - G_g)/G_a$, was ~0.06. The sensor sensitivity versus time for the fourth cycle is presented in Figure 4f. The response time and recovery time are ~20 s and ~4.5 min, respectively. These results confirm that as-produced CuO nanowires exhibit very useful gas sensing characteristics, where the sensitivity can be further optimized by reducing the NW size, tuning the defect and carrier concentrations, doping with an appropriate catalyst, and increasing the device operating temperature.

3.4. The Optoelectronic and Photoconduction Properties of CuO NWs. A dense array of CuO NWs were cleanly removed from the copper/(copper oxide) surface by gently pressing a thin piece (~1 mm) of polydimethylsiloxane (PDMS) against the top of the oxide, leaving the amorphous oxide layer intact (Figure 1a). The PDMS film with high density NWs covering the surface (Figure 5a) was directly used to perform UV−visible absorption measurements. The resulting transmittance spectrum is presented in Figure 5b. The long shallow absorption edge may be due to scattering effects of the randomly oriented NWs. Following the procedure outlined before,[31] $(\alpha \cdot h\nu)^2$ is plotted as a function of photon energy in Figure 5b

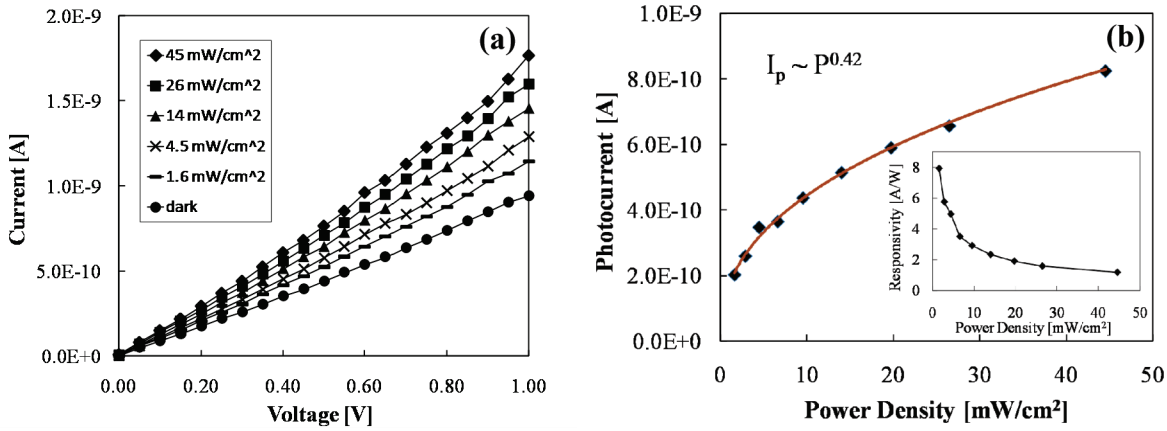

Figure 6. (a) Current−voltage ($I-V$) curves recorded for the CuO NW device in dark and various light intensities. (b) Photocurrent versus incident light intensity with power law fit. (Inset) Estimate of the photoconductive gain versus estimated photon flux of the irradiated NW.

(inset), where $h\nu$ is the photon energy and α is the absorption coefficient. By extrapolating the straight-line portion of the plot to the energy coordinate, one obtains an optical bandgap of ∼1.4 eV, which is consistent with the literature reporting a range in CuO bandgaps from 1.2−2.0 eV.[14] The CuO NW bandgap (∼1.4 eV) lies in the low end of the near-infrared (NIR) region (800−2500 nm) and makes it a good candidate for white light detection with some NIR capabilities.

The photoconducting properties of an individual CuO NW with a diameter of ∼225 nm and channel length of ∼12 μm were characterized by configuring the nanowire as a planar metal−semiconductor−metal sensor while performing light intensity and time response measurements. The current−voltage ($I-V$) curves recorded for the CuO NW device in dark and different light intensities are presented in Figure 6a. Figure 6b is a plot of the photocurrent, I_p ($I_p = I_{il} - I_d$) versus light intensity, where I_d is the dark current and I_{il} is the current of the device when illuminated with an incandescent light source. The conductance exhibits a relative change of 25 to 87% for light intensities of ∼1.62 to 45 mW/cm^2, respectively. The photocurrent is found to be power law dependent on the light intensity, that is, $I_p \sim P^{0.42}$, where P stands for the light power density. The obtained nonlinear response fits well with the theory of photoresponse which gives a power law dependence with an exponent of ∼0.5 for the high-injection case and a linear dependence for the low injection case.[32] Note that the device response remains Ohmic-like under dark and low illumination conditions, which points to the negligible role the contacts play on the transport in our devices. At the same time, the slightly non-Ohmic photo current−voltage characteristics obtained at high injection is due to the finite density of deep acceptor levels compared with the flux of incident photons.[32]

The device responsivity to white light, γ is derived from the data in Figure 6b. To calculate γ, the optical power absorbed by the device was calcualted by first estimating the absorption efficiency based on the following expression: $\eta = (1 - R)(1 - e^{-\alpha d})$, where R is the reflection coefficient of CuO, α is the absorption coefficient, and $d = 225$ nm is the effective thickness of the wire. Taking the average wavelength of the light source as ∼540 nm, $\alpha \approx 2 \times 10^5$ cm^{-1} and $R \approx 0.26$,[14] we obtain $\eta \approx 0.36$ for normal incidence and nonpolarized light conditions. The resultant values of γ as a function of the optical power densities is presented in Figure 6b (inset) with γ approaching ∼8 and 1 A/W for power densities of ∼1 and 45 mW/cm^2, respectively.

The large surface/volume ratio of NWs and the large number of surface defects combined with the short carrier transit times are well-known to strongly affect the sensing characteristics of NWs.[22,33,34] The strongly enhanced responsivity of CuO nanowire-based optical sensors obtained experimentally is likely to stem from combined effects of photocarrier multiplication inside the nanowire as well as carrier injection from the contacts and surface states for low incident intesities. More specifically, when the CuO NW is irradiated with light, additional electrons are made available for the chemisorption of O_2. The photoproduced electrons participating in chemisorption leave behind a paired hole that is then allowed to contribute to the conduction process. In addition, the chemisorbed oxygen has its usual effect of raising the conduction bands, which draws in additional holes from the electrodes. The decrease of the responsivity at relatively high light intensities is primarily attributed to electron-trap (chemisorption) saturation and e-h recombination. As the traps are filled with electrons, the quasi-Fermi level rises, resulting in the increased number of free electrons in the system, which in turn increases the probability of electron−hole recombination. A similar dependence has been found for photodetectors based on Si NWs and ZnO NWs.[33,34]

The electron trapping and chemical gating effect is further evidenced in Figure 7, where the NW device is irradiated with low intensity light (<1 mW/cm^2) during 100 ppm NO_2 gas detection. Upon exposure to NO_2 the current is found to increase by the chemisorption of NO_2 at the surface. When the current begins to plateau, white light was directed onto the sample through a chamber window. The current increases relatively sharply followed by a gradual plateau. Upon turning the light off, the current remains steady. The results confirm that photogenerated electrons participate in the absorption of molecules (NO_2 or O_2) at the surface which results in the availability of the paired hole for conduction, in addition to acting as a negative gate voltage. Furthermore, these results show that light irradiation onto a CuO NW sample during NO_2 detection can significantly enhance the response and offers an additional method to increase the gas sensing properties of p-type CuO NW devices. As a comparison, in the case of typical n-type metal oxide NWs light irradiation above the NW bandgap results in analyte desorption at the NW surface and in turn has been used to achieve faster recovery during NO_2 detection.[22]

The results of transient, on/off photoconduction measurements are additionally presented in Figure 8. The relatively slow recovery time (∼36 s) is due to the slow molecular desorption of the photoinduced, chemically absorbed oxygen molecules. The rising transient response is clearly defined by two regimes. The first regime is attributed to an intrinsic, that is, RC-circuit response, with little or no influence from traps. The second

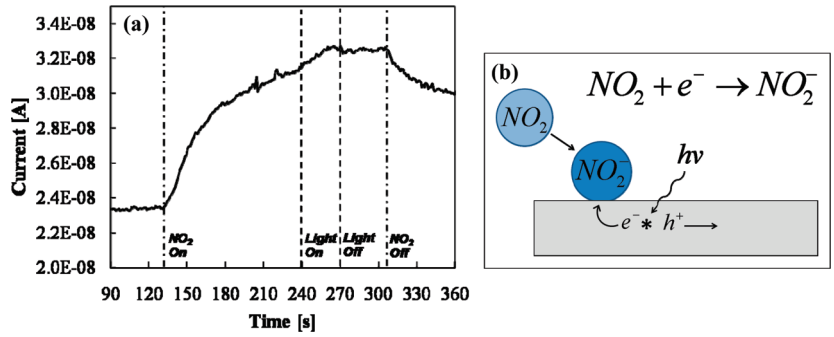

Figure 7. (a) The effect of light irradiation on the dynamic response of the CuO NW sensor for room-temperature detection of 100 ppm NO_2. (b) Proposed mechanism.

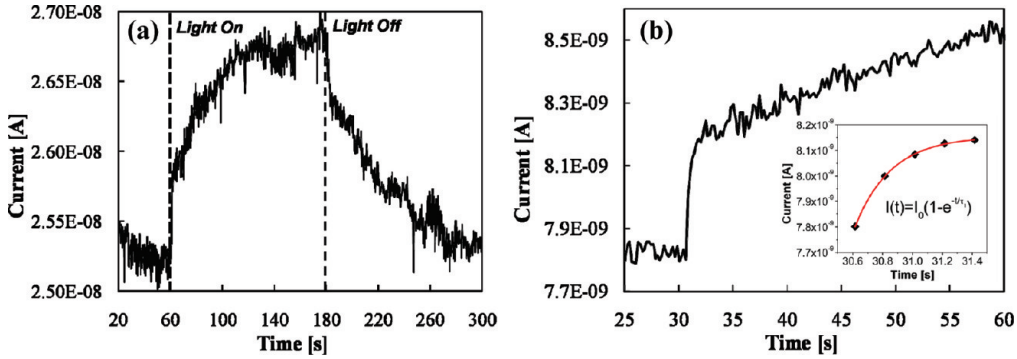

Figure 8. Time-resolved photoresponse of CuO NW device (biased at ~5 V) (a) and first leg of the time-resolved photoresponse of CuO NW device (biased at ~2 V) (b) with curve fit of the first regime (inset).

regime is characterized by a slow rise (nearly linear) and is a result of the complex interplay of different processes involving surface-assisted carrier recombination, trapping, and defect-assisted recombination/generation within the semiconductor. The two regimes are more clearly observed in Figure 8b. Fitting the first regime with a rising exponential decay of the form $I(t) = I_0(1 - e^{-t/\tau_1})$, a time constant of $\tau_1 = 240$ ms is obtained (inset of Figure 8b). The fast response holds promise for fast photosensing applications.

4. Conclusion

The large-scale and cost-efficient growth of ultrahigh dense CuO nanowire arrays has been achieved by a technically undemanding thermal oxidation of Cu substrates in an oxygen environment. According to FET and spectroscopic measurements, the as-grown nanowires are of p-type and feature a small bandgap of ~1.4 eV. The engineered metal−CuO−metal two-terminal NW devices showed strong and opposite electrical response to low concentrations of NO_2 and NH_3 gases with the primary mechanism being accumulation and depletion of holes within the main device region. The strong photoresponse to white light has been further obtained with the device responsivity levels approaching ~8 A/W for low power density of only ~1 mW/cm^2. The study opens a door to realizing a battery of advanced nano-opto-electronic devices based on individual p-type metal nano-oxides and their based p-n junctions for application in low-power IR−vis light sensors, optical switches, and gas-sensors.

Acknowledgment. J.H.C. acknowledges the financial support by National Science Foundation (CBET-0803142 and CMMI-0856753). X.Z. acknowledges the partial financial support by the National Science Foundation (ECCS-0802036, CMMI-0826191, ECCS-0901702, and CBET-0933653). SEM imaging was carried out at the UWM Electron Microscope Laboratory. TEM analyses were conducted in the UWM HRTEM Laboratory. The authors thank M. Gajdardziska-Josifovska for providing TEM access and D. Robertson for technical support with TEM analyses. The authors also thank the Photonics Center at Boston University.

References and Notes

(1) Xia, Y. N.; Yang, P. D.; Sun, Y. G.; Wu, Y. Y.; Mayers, B.; Gates, B.; Yin, Y. D.; Kim, F.; Yan, Y. Q. *Adv. Mater.* **2003**, *15*, 353.
(2) He, R. R.; Feng, X. L.; Roukes, M. L.; Yang, P. D. *Nano Lett.* **2008**, *8*, 1756.
(3) Lieber, C. M.; Wang, Z. L. *MRS Bull.* **2007**, *32*, 99.
(4) Kong, J.; Franklin, N. R.; Zhou, C. W.; Chapline, M. G.; Peng, S.; Cho, K. J.; Dai, H. J. *Science* **2000**, *287*, 622.
(5) Yang, R. S.; Qin, Y.; Dai, L. M.; Wang, Z. L. *Nat. Nanotechnol.* **2009**, *4*, 34.
(6) Hu, J. T.; Odom, T. W.; Lieber, C. M. *Acc. Chem. Res.* **1999**, *32*, 435.
(7) Park, W. I.; Kim, D. H.; Jung, S. W.; Yi, G. C. *Appl. Phys. Lett.* **2002**, *80*, 4232.
(8) Pan, Z. W.; Dai, Z. R.; Wang, Z. L. *Science* **2001**, *291*, 1947.
(9) Greene, L. E.; Law, M.; Tan, D. H.; Montano, M.; Goldberger, J.; Somorjai, G.; Yang, P. D. *Nano Lett.* **2005**, *5*, 1231.
(10) Hansen, B. J.; Lu, G. H.; Chen, J. H. *J. Nanomater.* **2008**, 830474.
(11) Jiang, X. C.; Herricks, T.; Xia, Y. N. *Nano Lett.* **2002**, *2*, 1333.
(12) Shen, G.; Chen, P. C.; Ryu, K.; Zhou, C. *J. Mater. Chem.* **2009**, *19*, 828.
(13) Collins, B. T.; Desisto, W.; Kershaw, R.; Dwight, K.; Wold, A. *J. Less−Common Met.* **1989**, *156*, 341.
(14) Ito, T.; Yamaguchi, H.; Masumi, T.; Adachi, S. *J. Phys. Soc. Jpn.* **1998**, *67*, 3304.
(15) Kouklin, N. *Adv. Mater.* **2008**, *20*, 2190.
(16) Nakamura, Y.; Yoshioka, H.; Miyayama, M.; Yanagida, H.; Tsurutani, T.; Nakamura, Y. *J. Electrochem. Soc.* **1990**, *137*, 940.
(17) Akimoto, K.; Ishizuka, S.; Yanagita, M.; Nawa, Y.; Paul, G. K.; Sakurai, T. *Sol. Energy* **2006**, *80*, 715.
(18) Liao, L.; Zhang, Z.; Yan, B.; Zheng, Z.; Bao, Q. L.; Wu, T.; Li, C. M.; Shen, Z. X.; Zhang, J. X.; Gong, H.; Li, J. C.; Yu, T. *Nanotechnology* **2009**, *20*, 085203.

(19) Wang, C.; Fu, X. Q.; Xue, X. Y.; Wang, Y. G.; Wang, T. H. *Nanotechnology* **2007**, *18*, 145506.
(20) Chen, J. J.; Wang, K.; Hartman, L.; Zhou, W. L. *J. Phys. Chem. C* **2008**, *112*, 16017.
(21) Zhu, Y. W.; Yu, T.; Cheong, F. C.; Xui, X. J.; Lim, C. T.; Tan, V. B. C.; Thong, J. T. L.; Sow, C. H. *Nanotechnology* **2005**, *16*, 88.
(22) Kolmakov, A.; Moskovits, M. *Annu. Rev. Mater. Res.* **2004**, *34*, 151.
(23) Yuan, G. D.; Zhang, W. J.; Jie, J. S.; Fan, X.; Zapien, J. A.; Leung, Y. H.; Luo, L. B.; Wang, P. F.; Lee, C. S.; Lee, S. T. *Nano Lett.* **2008**, *8*, 2591.
(24) Martel, R.; Schmidt, T.; Shea, H. R.; Hertel, T.; Avouris, P. *Appl. Phys. Lett.* **1998**, *73*, 2447.
(25) Fan, Z. Y.; Wang, D. W.; Chang, P. C.; Tseng, W. Y.; Lu, J. G. *Appl. Phys. Lett.* **2004**, *85*, 5923.
(26) Lu, G. H.; Ocola, L. E.; Chen, J. H. *Adv. Mater.* **2009**, *21*, 2487.
(27) Zhang, K. L.; Rossi, C.; Tenailleau, C.; Alphonse, P.; Chane-Ching, J. Y. *Nanotechnology* **2007**, *18*, 145506.
(28) Haugsrud, R. *J. Electrochem. Soc.* **2002**, *149*, B14.
(29) Göpel, W. *Sens. Actuators, A* **1996**, *56*, 83.
(30) Wagh, M. S.; Jain, G. H.; Patil, D. R.; Patil, S. A.; Patil, L. A. *Sens. Actuators, B* **2006**, *115*, 128.
(31) Omari, M.; Kouklin, N.; Lu, G.; Chen, J.; Gajdardziska-Josifovska, M. *Nanotechnology* **2008**, *19*, 105301.
(32) Sze, S. M.; Ng, K. K. *Physics of Semiconductor Devices*, 3rd ed.; John-Wiley & Sons, Inc.: Hoboken, NJ, 2007.
(33) Zhang, A.; You, S. F.; Soci, C.; Liu, Y. S.; Wang, D. L.; Lo, Y. H. *Appl. Phys. Lett.* **2008**, *93*, 121110.
(34) Soci, C.; Zhang, A.; Xiang, B.; Dayeh, S. A.; Aplin, D. P. R.; Park, J.; Bao, X. Y.; Lo, Y. H.; Wang, D. *Nano Lett.* **2007**, *7*, 1003.

JP908850J